GCM Simulations of the Climate in the Central United States

Kenneth E. Kunkel and Xin-Zhong Liang

Illinois State Water Survey

Champaign, Illinois

Abstract

A diagnostic analysis of relationships between central United States climate characteristics and various flow and scalar fields was used to evaluate 9 global coupled ocean-atmosphere general circulation models (CGCMs) participating in the Coupled Model Intercomparison Project (CMIP). In order to facilitate identification of physical mechanisms causing biases, data from 21 models participating in the Atmospheric Model Intercomparison Project (AMIP) were also used for certain key analyses.

Most models reproduce basic features of the circulation, temperature, and precipitation patterns in the central US, although no model exhibits small differences from the observationally-based data for all characteristics in all seasons. Model ensemble means generally produce better agreement with the observationally-based data than any single model. A fall precipitation deficiency, found in all AMIP and CMIP models except HadCM3, appears to be related in part to slight biases in the flow on the western flank of the Atlantic subtropical ridge. In the model mean, the ridge at 850 hPa is displaced slightly to the north and to the west, resulting in weaker southerly flow into the central US.

The CMIP doubled-CO_2 transient runs show warming (1-5°C) for all models and seasons and variable precipitation changes over the central U.S,. Temperature (precipitation) changes are larger (mostly less) than the variations that are observed in the 20th Century and the model variations in the control simulations.

1. Introduction

The coupled ocean-atmosphere general circulation models (CGCMs) that are the principal tools for assessment of potential anthropogenically-forced climate change exhibit a sizeable range of global sensitivities for temperature and precipitation. While global changes in key elements such as temperature and precipitation are important for some societal impacts (e.g. sea level rise), many of the potential impacts result from local and regional changes in climate. Such regional changes may differ substantially from zonally-averaged changes in the climate system, as has been observed in the recent past where the southeastern U.S. has cooled slightly since 1900 while most other Northern Hemisphere land areas have warmed (Folland et al. 2001). Furthermore, the uncertainties on a regional scale are greater than those on a global scale. These regional uncertainties are critical for assessing the impacts of future climate change and evaluating management strategies and policy options.

The Atmospheric Model Intercomparison Project (AMIP; Gates et al. 1998) and the Coupled Model Intercomparison Project (CMIP; Meehl et al. 2000), through their controlled experiments and worldwide participation of modeling groups, have proven to be very effective at improving understanding of uncertainties in model projections. Most assessments have taken a global perspective (e.g. Barnett 1999; Lambert and Boer 2001; Covey et al. 2003). This needs to be the primary focus since global circulation systems must be simulated correctly to produce reasonable regional climates. However, regional analyses are also valuable. Regional geographic/topographic features often have substantial influences on the regional climate but little influence globally. Furthermore, such analyses can illuminate inconsistencies in large-scale circulation patterns that may be minor on a global scale, but important to some regions. Insights gained in this manner can be used to choose appropriate models for climate change assessments.

For example, in a regional study of the Saharan desert Liu et al. (2002) analyzed 18 CMIP model simulations and identified the 5 models closest to the present-day climatology based on area of desert (annual precipitation < 50 mm), areally-averaged precipitation within the desert, and location of the boundaries of the desert. For these 5 models, desert area was within 25% of observed, desert-averaged precipitation was within 10 mm of observed, and the boundaries of the 50 mm isoline were judged to be close to observed. These 5 models were then used to assess the sensitivity of the Saharan climate to increasing global concentrations of greenhouse gases.

The principal objective of this study is to assess the ability of CGCMs to simulate the climate of the central United States, with a focus on precipitation. A general approach to a comprehensive assessment will involve several levels. At a basic level, an assessment will examine climatological mean fields. Higher level analyses might include examination of the frequency and intensity of extreme events and of temporal variations and trends. The latter is particularly interesting, but challenging for models, because of the observed regional variations in long-term trends. This study is a first step and thus concentrates on the climatological mean fields.

In order to illuminate the possible physical basis for model biases, an approach was used here that goes somewhat beyond the standard model intercomparison study and follows that of Liang et al. (2001b). First, observed interannual variability patterns were used to establish physical links between surface climate elements and flow patterns and to identify key areas for definition of indices. Then, ensembles of model simulations were used to identify systematic relationships among model biases and explain their occurrence.

The region of study ("CUS"; delineated in Fig. 1) is part of one of the most productive agricultural regions in the world. It includes several major urban areas (notably Chicago, the

third largest in the US) and a portion of the drainage basin of the North American Great Lakes. Although precipitation is substantial (region-wide average annual precipitation is 980 mm), increasing population and economic growth may cause water shortages in the future. In the global depictions of CMIP results by Covey et al. (2003), this region is not highlighted as one where the simulated control climate exhibits large deviations from the observed climatology. The present analysis is more detailed, examining more fields and addressing the seasonal cycle.

Most precipitation in the central U.S. is associated with the passage of extratropical cyclones (ECs); this is the case in all seasons, although in the warm season other features (e.g. heating-induced instability, mesoscale convective systems) make some contribution. Thus, the location and the temporal variability of the mid-latitude upper-level jet stream are important climate features for this region. The Great Plains southerly low-level jet is another key feature, especially in summer. For the central US, Mo and Higgins (1996) indicated that the most important source of water vapor is transport from the Gulf of Mexico via southerly wind flow in all seasons. A more in-depth study of summer using a water vapor tracer diagnostic technique (Bosilovich and Schubert 2002) showed that the actual source regions of water vapor include more distant areas such as the tropical and western Atlantic. Their results also indicated that the contribution from the Pacific Ocean is small, a consequence of rain shadowing by the several mountain ranges to the west. Land surface evaporation was found to be important, particularly local recycling and flow from the southeast U.S. However, this is a rather small reservoir that must be regularly replenished by oceanic sources. Dirmeyer and Brubaker (1999) compared moisture sources for two contrasting years, 1988 and 1993, and showed that the main difference was increased moisture transport in 1993 from the western Gulf of Mexico and the Carribean Sea. Based on the above considerations, our diagnoses focused on the upper level jet and the

Great Plains low-level jet to assess and understand the performance of GCMs, including their climate biases as compared with observationally-based data and inter-model differences. The primary emphasis is on results from CMIP models since fully-coupled models are used to develop climate change projections. However, analysis of AMIP model data was also performed and selected AMIP results are included to help better understand the model biases.

2. Data

The Atmospheric Model Intercomparison Project (AMIP, Gates et al. 1998) was undertaken to provide a framework for comparisons of atmospheric GCMs (AGCMs). The AMIP experiment analyzed in this study was an historical simulation of the period 1979-1995. The sea surface temperatures (SSTs) were specified as monthly mean variations based on actual observations. In this experiment, all AGCMs use the same ocean surface conditions to determine the fluxes of heat, moisture, and momentum needed to drive the atmosphere. The SST boundary conditions were prepared for this experiment (details found at http://www-pcmdi.llnl.gov/amip/AMIP2EXPDSN/BCS/amip2bcs.html) based on the Hadley Centre SST data set (version GISST2.2a) of Rayner et al. 1996 and the optimal interpolation SST (OISST version 1) data set of Reynolds and Smith (1994). Each model also used the same values of atmospheric CO_2 concentration (345 parts per million) and solar constant (1365 W m^{-2}). Specification of the land surface and inclusion of the radiative effects of other greenhouse gases and aerosols was left up to each modeling group and thus varied among models. Data from this experiment include 21 AGCMs.

The Coupled Model Intercomparison Project (CMIP, Meehl et al. 2000) is similar to AMIP except that the models are fully coupled GCMs. The experiment analyzed in this study is denoted as "CMIP2". This consisted of a control run of at least 80 years duration in which

greenhouse gas concentrations were fixed followed by a transient run of at least 80 years duration in which CO_2-equivalent concentration increased at the rate of 1%/year. A variety of methods were used to determine the initial state of the atmosphere and ocean at the beginning of the control run; these are briefly described at http://www-pcmdi.llnl.gov/modeldoc/cmip/table2.html. In both runs, the solar constant and land use did not change and the inclusion of aerosol effects and other greenhouse gases varied among models. In the transient run, CO_2-equivalent concentrations reach a doubling compared to initial concentrations around year 70. Data from this experiment include 9 CGCMs. Several of the models participating in both AMIP and CMIP use the same or a very similar atmospheric component. The particular dataset used in the present study is referred to as "CMIP2+" which is an extension of CMIP2 with an expanded set of fields at monthly or shorter time resolution.

Table 1 lists the CMIP CGCMs used in this study along with certain model characteristics and key references. Since these models contain an interactive ocean component and ocean surface conditions are computed by the model rather than specified, the SSTs can differ among models and from observations. Six models use flux adjustment to minimize climate drift while the other three do not.

There are some differences between the CMIP and AMIP experiments. In the AMIP experiment, the CO_2-equivalent concentration was fixed at 345 ppm for all models while in the CMIP control simulation it varied among the models from 290 to 360 ppm. Likewise, the solar constant was fixed in AMIP at 1365 W m^{-2} while in CMIP it varied among models from 1365 to 1370 W m^{-2}.

The differences in forcing, particularly from CO_2 concentration differences, among CMIP models is a factor to be considered in interpreting the results. For convenience, a common

historical period (1979-1995) is used for comparison of the control simulations, but the average CO_2 concentration in that period (349 ppm) is substantially higher than in several of the control simulations and slightly lower than in others. In addition, the actual forcing during 1979-1995 is transient and the climate system is not in equilibrium, unlike the control simulations. Also, time-varying aerosol concentrations, land-cover, and other factors may have some measurable effects on the observational record. Since the control simulations are idealized, it is highly likely that some model-observation differences are not due to model deficiencies, but to these forcing differences. Although it is not possible to separate these effects, where appropriate analyses were performed to identify possible relationships between CO_2 concentrations and model biases.

All model data were obtained through the web-based infrastructure of the Program for Climate Model Diagnosis and Intercomparison. Two major sources of data for validation were used: (1) the NCEP-DOE AMIP II reanalysis (R-2; Kanamitsu et al. 2002) for comparison of wind, humidity and pressure patterns, and (2) data from the National Weather Service's cooperative observer network (COOP), as archived in the TD-3200 data set of the National Climatic Data Center, for comparison of surface air temperature and precipitation.

3. Results

Various climate elements were available as monthly means at each grid point with varying grid spacings. The following climate elements were chosen for diagnostic analysis: precipitation, surface air temperature, wind and pressure level height at 850 and 200 hPa, and specific humidity (q) at 850 hPa. The analysis at 850 hPa was chosen because much of the moisture transport into the central US from the Gulf of Mexico occurs at and below this level. The analysis at 200 hPa was chosen because this level is near the core of the upper level jet stream.

In the following discussion, the R-2 fields are first presented; these provide the basis for the diagnostics presented in some of the graphs. This is followed by an analysis of precipitation and temperature in the control simulations. Finally, a brief analysis of temperature and precipitation changes in the transient simulations is presented.

a. Reanalysis fields

Figure 2 shows average flow patterns at 850 and 200 hPa from R-2. At 850 hPa, the average winter flow in the central US is westerly to northwesterly. Because flow from the Gulf of Mexico does not often penetrate into the central US, the winter season is relatively dry. During the spring, summer, and fall, the mean flow is still westerly, but it is part of a curved pattern that originates in the Gulf of Mexico, moves across Texas, and curves northeastward into the central US. Thus, moisture is more abundant in these three seasons. This pattern is most pronounced in the summer, the wettest season.

At 200 hPa, the average flow is westerly over the central U.S in all seasons. The average position of the jet stream is to the south of the central US in winter and spring, over the region in fall, and to the north in summer. Highest wind speeds occur in the winter when the north-to-south temperature gradient is largest.

An analysis was undertaken in which a time series of monthly precipitation anomalies averaged for the central US region was correlated with time series of the meridional wind component at 850 hPa for each grid point. Maps of the spatial pattern of correlations (Fig. 3) show that precipitation anomalies are highly correlated with southerly flow over the Mississippi River basin at 850 hPa. Correlations of greater than 75% are seen for distinct broad areas. There are slight variations by season with a westward shift in the pattern in the summer. However, high correlations are seen in all seasons from central Texas to Louisiana.

A similar analysis was performed for the zonal wind component at 200 hPa. High correlations are found generally in a belt from California to the Great Lakes (Fig. 3). This reflects the average location of the jet stream during periods when extratropical cyclones are causing precipitation over the central U.S. There are some seasonal variations in the strength of the correlations, but the location of the high correlations is about the same in all seasons, although correlations in the central US are quite low in the fall.

The results shown in Fig. 3 were used to identify 2 regions (Fig. 1) for defining indices in the analysis of the model data. Although all seasons were considered, the summer season was given the highest weight because of its importance to the widespread non-irrigated agriculture of the region. The box covering eastern Texas and Oklahoma corresponds to an area of high correlations at 850 hPa and reflects the importance of low level moisture transport from the Gulf of Mexico; this area will be referred to as the "LLJ" (low level jet) region. As shown in Figs. 2 and 10, this is the actual low level jet (high wind speed) region, both in the R-2 data and in a model mean depiction. An examination of individual model maps indicates that high 850 hPa wind speeds are found in this area for all models. The box covering Iowa and portions of adjacent states corresponds to an area of high correlations at 200 hPa in winter, spring, and summer; this will be referred to as the "UJ" (Upper-Level Jet) region.

b. Model precipitation

Annual and seasonal precipitation for the control runs of CMIP models and for the COOP data is shown in Fig. 4 for the CUS region (Fig. 1). In the CMIP control runs, the SSTs are calculated by the model and the CO_2 concentration is fixed. As noted before, no common historical observational period will match the model forcing for all model simulations. In the case of the AMIP simulations, the SSTs are specified from the period 1979-1995 and thus a

direct comparison with the COOP and R-2 data for that same period is appropriate. For convenience, we have chosen the same 1979-1995 period for comparison with CMIP results. Model values of annual mean precipitation range from 2.0 to 3.2 mm d^{-1}, compared to a COOP value of 2.7 mm d^{-1}. The model mean value is 2.6 mm d^{-1}. Seven of the 9 models are within 10% of the COOP data. The CSIRO is about 25% drier than COOP and the HadCM3 is about 20% wetter. The comparison of seasonal precipitation indicates some inconsistencies across seasons. In winter, all models are within 25% of the COOP data except for HadCM3 which is about 50% wetter than COOP. In spring, all models are close to, or wetter than, COOP. The GFDL and HadCM3 are more than 20% wetter than COOP. In summer, 5 of the 9 models were within 10% of COOP. The CSIRO and GFDL are 20% or more drier than COOP, while the PCM and CSM are about 15% wetter than COOP. All models but one are substantially drier than COOP in fall, the only exception being the HadCM3. The CMIP model mean values are very near the COOP values, except for fall (model mean of 2.0 mm d^{-1} compared to a COOP value of 2.8 mm d^{-1}). A graph of model biases versus the control CO_2 concentrations (not shown) did not indicate any systematic relationship, suggesting that the effect of different forcing is probably small relative to other sources of biases.

The negative bias in fall precipitation exhibited by 8 of the 9 CMIP models is also found in the AMIP experiment (Fig. 4). All 21 AMIP models exhibit a negative bias and the AMIP model mean is 1.8 mm d^{-1}. Thus, this model bias presumably originates in the atmospheric component.

Moisture transport was investigated by examining 850 hPa data. An analysis of 17 years (1979-1995) of radiosonde data for Oklahoma City, located in the LLJ region, indicated a high correlation (r=0.91) between monthly averages of v_{850} and vertically integrated qv. Thus, the v

component of the 850 hPa wind was used as a simple surrogate for moisture transport. A comparison of the southerly component of the 850 hPa wind speed in the LLJ region for CMIP models and R-2 data (Fig. 5a) indicates that all models produce the correct seasonal cycle with a maximum in the summer and a minimum in the winter. The amplitudes of the seasonal cycle are similar to the R-2 data for many models. One notable exception is ECHO whose seasonal amplitude of 1.6 m s^{-1} is much less than the R-2 value of 4.8 m s^{-1}. Both CCCMA and HadCM2 have somewhat larger amplitudes than R-2. The model mean values are very close to R-2 in spring and summer, slightly more negative in winter, and smaller in fall. The weaker southerly flow in fall may be related to the negative precipitation biases.

For specific humidity at 850 hPa in the LLJ region (Fig. 5b), the CMIP models generally simulate the seasonal cycle with a minimum in winter and a maximum in summer. Although magnitudes are generally within 15% of the R-2 data, the CCCMA and HadCM3 are more than 15% moister in spring, summer and fall. The model mean values are very close to R-2 in all seasons.

Interannual correlations between CUS precipitation and the southerly wind component at 850 hPa in the LLJ region were calculated for CMIP models by season (Fig. 6a). The values for the models are within 20% (this is the absolute, not relative, difference, the convention used here for all correlation graphs) of R-2/COOP in the winter except for HadCM2. In the spring, three models (ECHO, PCM, and HadCM2) differ from R-2/COOP by more than 30%. In summer, CCCMA, HadCM2, and HadCM3 differ from R-2/COOP by more than 40%. In fall, the ECHAM4 differs by about 40% and HadCM2 by about 55%. The model mean values are lower than R-2/COOP in all seasons, most notably in summer and fall.

Interannual correlations for the UJ region between CUS precipitation and the westerly wind component at 200 hPa are shown in Fig. 6b for CMIP models. In winter, CSM and HadCM2 differ from the R-2/COOP correlation by more than 20%. In spring, ECHO is about 40% lower than R-2/COOP. In summer, all models have somewhat lower correlations than R-2/COOP. In fall, all correlations are within 20% of R-2/COOP. The model mean values are relatively close to R-2/COOP except for summer where the model mean value of 36% is considerably smaller than the R-2/COOP value of 68%.

c. Model temperature

The comparison of mean annual temperature in CMIP models (Fig. 7) indicates that all models are within 1.5°C of the 1979-1995 COOP mean. Model values range from 9.1 to 12.3°C. The model mean value of 10.4°C compares favorably with the COOP value of 10.7°C. Somewhat larger differences are observed for the seasonal values (Fig. 7), although the amplitude of the seasonal cycle is similar to COOP for most models. The HadCM3 and CSIRO models exhibit a somewhat larger amplitude in the seasonal cycle with colder temperatures in the winter and warmer temperatures in the summer compared to the COOP data. The CCCMA model exhibits very cold temperatures (about 5°C less than COOP) in the spring, but is within 2°C of COOP in the other 3 seasons. The model mean shows a seasonal cycle whose amplitude is slightly larger (by 1.3°C) than COOP, a result consistent with Covey et al. (2000). As was the case for precipitation, a graph of model biases versus CO_2 concentrations (not shown) did not indicate any systematic relationship, suggesting that the effect of different forcing is probably small relative to other sources of biases.

The AMIP model mean temperature is slightly larger (1-2°C) than the CMIP model mean in each season. Also, some AMIP models are warmer than any of the CMIP models. Although the cause of the warmer temperatures in the AMIP simulations is not obvious, the AMIP models were driven by SST boundary conditions from the relatively warm 1979-1995 period, during which global CO_2 concentrations rose from 336 to 361 ppm. By contrast, the average CO_2 concentration of the CMIP control simulations was 338 ppm, similar to the very early part of the AMIP period.

d. Model Sensitivity to Enhanced Greenhouse Gas Forcing

The sensitivity of CMIP models to selected changes in forcing was analyzed by examining years 65-75 in the transient simulation and comparing precipitation rates and temperatures for this period with the last 30 years of the control simulation. Seasonal results are presented in terms of differences between the two periods (Fig. 8 and 9). Since the CO_2 concentrations in the control simulations differ among models, a 1% annual change translates into an absolute rate of concentration change, and therefore forcing rate of change, that differs among models; the CO_2 concentrations in Year 70 of the transient simulations is listed in Table 1. As a result, differences in temperature and precipitation changes may not be due entirely to differences in model sensitivity.

For precipitation (Fig. 8), in winter 5 of the 9 models show little change while the other 4 exhibit increases of 0.2-0.4 mm d^{-1}. In spring, 4 of the 9 models show changes of less than 0.2 mm d^{-1} while the other 5 exhibit increases of 0.2-0.5 mm d^{-1}. There is more variability in summer. The ECHO and ECHAM4 show increases of more than 0.2 mm d^{-1}. By contrast, the CCCMA, HadCM2, and HadCM3 show sizeable decreases of 0.6 mm d^{-1}. In fall, 6 of the 9 models show changes of less than 0.2 mm d^{-1} while 3 show decreases of more than 0.2 mm d^{-1}.

How do these changes compare to precipitation variations that would occur naturally, that is, without enhanced greenhouse warming? This question was investigated by performing a more detailed analysis of the control simulations of the CMIP models. The length of the control simulation varied among models, but was at least 79 years in length. Time series of seasonal precipitation were smoothed with an 11-year running average filter. The maximum, minimum, and mean values among these running windows were identified and the range expressed as a difference from the mean was plotted in Fig. 8. The smoothing window of 11 years was chosen to match the length of the analyzed portion of the transient simulation. A similar analysis was performed on COOP data for the period 1900-1999. The maximum and minimum values are in the range of 0.2-0.6 mm d^{-1} above and below the mean for both models and the COOP data except for HadCM2 in the summer with values of 0.8 mm d^{-1}. When comparing these variations to the transient changes shown in Fig. 8, in most cases the transient changes are within the envelope of the natural variations. These results suggest that the transient simulations' changes due to the specified anthropogenic forcing are in most cases not clearly different from variations observed in the 20th Century or simulated in the control runs. Since the CMIP models use somewhat different values of CO_2 concentration in their simulations, perhaps the differences among models is due in part to this factor. However, a graph of precipitation changes versus CO_2 concentration (not shown) did not indicate any systematic relationship, suggesting that the model differences are not primarily due to differences in CO_2 greenhouse gas forcing. Also, there were no systematic relationships between precipitation changes and the control simulation biases documented in Figs. 4-7.

Another issue of interest is the relationship, if any, of the regional changes to global changes. This was explored by comparing the results of this study to those of Covey et al.

(2003), who presented time series of global annual temperature and precipitation for the transient simulations out to Year 80. The ECHO model was not included in the Covey et al. (2003) study. Excluding ECHO, the CUS region precipitation changes in Fig. 8, averaged annually to compare with the Covey et al. (2003) results, range from about -0.30 to +0.15 mm d^{-1}. The range of global changes is -0.02 to +0.12 mm d^{-1}, or a factor of 3 smaller. The models with the largest positive changes globally are GFDL and CSIRO, but for CUS these show little change and are intermediate among the rest of the models. Two models with large negative changes for the CUS region-CCCMA, CSM and HadCM3-are also on the low end of global changes with values of less than +0.04 mm d^{-1}, but another with large CUS negative changes, CSM, is intermediate among models in global precipitation changes. Thus, there does not appear to be a relationship between the regional and global changes.

For temperature (Fig. 9), all models show warming in all seasons, but there is considerable variation in the magnitude. The seasonal ranges are about +1 to +5°C in winter, +0.6 to +5.4°C in spring, +0.8 to +5.0°C in summer, and +1.7°C to +4.0°C in fall. As was done for precipitation, an 11-yr running average filter was applied to the temperature time series of the control simulations to examine the internal variations of the models and to COOP temperatures for 1900-1999. The maximum and minimum values of the 11-yr running average time series, expressed as a difference from the average, indicate variations about the average of 0.4-1.4°C for both models and the COOP data. Most, but not all, of the temperature increases found in the transient simulations exceed the range of internal model variations found in the control simulations and COOP variations, suggesting that warming in these models is clearly due to the models' anthropogenic forcing. As exceptions, the summer warming in the PCM is slightly less than the COOP range and the spring warming in the CSM is slightly less than its own internal

variability. As was the case for precipitation, a graph of precipitation changes versus CO_2 concentration (not shown) did not indicate any systematic relationship, suggesting that the model differences are not primarily due to differences in CO_2 greenhouse gas forcing. Also, there were no systematic relationships between temperature changes and the control simulation biases documented in Figs. 4-7.

The range of global changes in Covey et al. (2003) is about +1.3C to +2.2C. The regional changes, averaged annually, range from +1.3C to 4.4C, a range that is about 3 times larger than the global range. Unlike precipitation, there is some consistency in the regional vs global changes. The models with largest regional changes, the CCCMA and HadCM3, are on the upper range of global changes, while the models with the smallest regional changes, the CSM and PCM, are on the lower end of the range of global changes.

4. Discussion

There is considerable model-to-model variability in the GCMs' simulations of the regional climate of the central US. For precipitation-related variables, most models reproduce certain basic features of the regional climate. The general shape of the seasonal cycle is simulated. Most models are able to simulate the seasonal changes in southerly flow from the Gulf of Mexico and the atmospheric water vapor content there and in the central US. These results reflect the models' ability to reproduce the large-scale circulation patterns and basic processes of the hydrologic cycle. There is more variation among the models in reproducing the connections between specific circulation patterns and precipitation episodes in the central US.

Model mean (averages of all models; MM) maps were produced to provide additional insights. Both Lambert and Boer (2001) and Covey et al. (2003) presented global MM maps of

selected fields for CMIP simulations. The MM maps for 850 hPa and 200 hPa flow for the 30-year control CMIP period (Fig. 10) are in impressively close correspondence with the R-2 patterns (Fig. 2). This is similar to the global scale results of Lambert and Boer (2001) who found that the model mean provided an overall best comparison with climatology. However, there are subtle differences that may be important for precipitation processes in the central US. In the winter, the minimum 850 hPa wind speed in the Gulf of Mexico extends further to the west to the Texas coast. In the spring, the 850 hPa comparison is quite close. In the summer, the 850 hPa minimum is shifted to the east and the high wind speed core over Texas is weaker and broader compared to R-2. This may explain in part the more variable correlation patterns in the models (Fig. 6a). In the fall, the 850 hPa minimum is shifted to the north and extended to the west. This shift in the fall may explain the low precipitation because the MM pattern would lead to an overall weaker advection of moisture from the Gulf of Mexico. Interestingly, Gutowski et al. (2004) and Liang et al. (2004) independently ran regional climate simulations, driven by R-2 data, of the observed climate and found fall precipitation deficiencies in the lower Mississippi River basin extending into the central U.S; thus, this fall bias is not limited to global models. At 200 hPa, the location of the spring maximum wind speed is slightly to the north of R-2. In summer, the 200 hPa wind speed maximum is somewhat higher than R-2. The 200 hPa comparison for fall and winter is quite close.

The similarity of AMIP and CMIP results suggests that precipitation biases are principally a consequence of atmospheric processes. To explore these biases further, an analysis of AMIP model data was undertaken. Only AMIP results are presented because the larger number of models provides a more robust statistical description. For each AMIP model, monthly mean maps of 850 hPa southerly and 200 hPa westerly wind flow biases (model mean minus R-

2) were prepared, resulting in a total of 252 (12 months x 21 AMIP models) maps for each level. To examine whether model precipitation biases are systematically related to flow biases, each monthly map and associated monthly mean model precipitation bias for the CUS region is treated as a sample. For each grid point and each season, a correlation coefficient was calculated for the 63 (21 models x 3 months) data pair samples. Maps of the correlation coefficients (Fig. 11) show interesting patterns that provide possible insights. At 850 hPa (Figs. 11a-d), there are sizeable areas of statistically significant positive correlations, indicating that there is a tendency for the wetter (drier) models to be characterized by stronger (weaker) southerly flow. During winter, spring, and fall (Figs. 11a,b,d), these are located from the Gulf of Mexico extending into the central U.S. In the summer, the area is further east. It is interesting to compare with the correlation maps between COOP precipitation and R-2 wind shown in Fig. 3, even though the Fig. 11 maps show correlations among models for climatological mean biases while Fig. 3 show interannual correlations in the R-2/COOP data. Liang et al. (2001a) made a similar comparison to identify physical mechanisms for GCM biases in simulating the China monsoon system. For winter, spring, and fall, the positive correlations in Fig. 11 are located in the same general regions as found for the R-2/COOP correlation maps (Fig. 3). For summer, the high correlation area in the eastern portion of the central US (Fig. 11c) is in the same area as R-2/COOP high correlations (Fig. 3c), but the correlations are near zero over Texas, an area of high correlations in the R-2/COOP map (Fig. 3c). At 200 hPa, the winter, spring, and fall (Fig. 11e,f,h) maps show statistically significant positive correlations over the eastern subtropical Pacific and negative correlations over the northwest US. This indicates that the wetter (drier) models are characterized by enhanced (decreased) baroclinicity over the eastern subtropical Pacific and decreased (enhanced) baroclinicity over southwest Canada. For summer (Fig. 11g), there is an

area of positive correlations over the central U.S., indicating that the wetter (drier) models are characterized by enhanced (decreased) baroclinicity in the central U.S. By comparison, the R-2/COOP correlation maps (Fig. 3e-h) show that in all seasons, wetter (drier) months are characterized by enhanced (decreased) baroclinicity in the central U.S.

The results presented in Fig. 11 suggest that the model biases in precipitation are related in part directly to biases in simulation of the low level flow regimes and these relationships occur in similar regions where observed flow variations are correlated with observed CUS precipitation variations. One notable exception is the LLJ region in summer. Although there are sizeable differences in LLJ 850 hPa southerly flow among the models (see Fig. 5a), these do not relate to model precipitation biases. Of course, there are other potential sources of biases not directly represented by flow patterns. For example, the mountain chains in the western US play an important role in key features such as the LLJ, especially in summer, and the development and path of ECs. The topographic variations in GCMs are a rather crude approximation of reality because of their coarse spatial resolution. In addition, the parameterization of the precipitation processes occurring within a grid box is known to be one of the most challenging aspects of climate system modeling because many processes, such as individual thunderstorm cells, are of a much smaller scale than the size of a grid, yet are extremely important to the magnitude of precipitation.

5. Conclusions

This analysis, primarily focused on precipitation, used diagnostic relationships between surface climate characteristics and various flow and scalar fields as the basis for model evaluation. This evaluation included qualitative descriptions of the comparison between models

and the R-2 and COOP data for geographical distributions of various key variables. In addition, indices of flow and water vapor content were calculated for several key regions and correlated with precipitation anomalies in the central US to provide a concise quantitative measure of model performance and better understanding of model biases.

In general, the CMIP models reproduce basic features of the circulation, temperature, and precipitation patterns in the central US, including the pronounced seasonal cycles that are characteristic of this region and the general flow patterns, although no model exhibits small differences from the R-2 and COOP data for all characteristics in all seasons. Similar to the findings of other investigators performing global analyses, model ensemble means generally produce better agreement with R-2 and COOP data than any single model. No single model is unambiguously superior to all other models. Among CMIP models, the CSIRO and HadCM3 models exhibit the largest precipitation biases. The HadCM3 is also the coolest CMIP model.

The fall precipitation deficiency, common to all AMIP and CMIP models except HadCM3, appears to be related in part to slight biases in the flow on the western flank of the Atlantic subtropical ridge. In the model mean, the ridge at 850 hPa is displaced slightly to the north and to the west, resulting in weaker southerly flow into the central US. By contrast, fall dry biases found by Gutowski et al. (2004) in regional climate model simulations did not appear to be related to circulation biases. They suggested that local water recycling may be responsible, an effect not investigated here. A full explanation of the responsible physical mechanisms for this feature remains a challenging problem.

The range of model changes (transient-control) due to increasing CO_2 concentrations is about 3 times larger for the CUS region than for the globe as a whole, both for temperature and precipitation. The regional changes are somewhat consistent with global changes for

temperature, that is, the models with greater global sensitivity give larger regional changes. However, there is little consistency between regional and global changes for precipitation.

6. Acknowledgements

This work was partially supported by the Illinois Board of Higher Education (IBHE) and the United States Environmental Protection Agency (USEPA) under award number EPA RD-83096301-0. Data analysis and graphics preparation were performed by Li Li and Heng Liu. We are grateful to the participating CMIP2+ model groups for generously making their data sets available, including George Boer (Canadian Centre for Climate Modeling and Analysis, Victoria Canada), Bill Collins (National Center for Atmospheric Research, Boulder, CO USA), Curt Covey (Program for Climate Model Diagnosis and Intercomparison, Lawrence Livermore Laboratory, Livermore, CA USA), Jonathan Gregory (Hadley Centre for Climate Prediction and Research, UK Met Office, Bracknell, Berkshire, United Kingdom), Tony Hirst (CSIRO Division of Atmospheric Research, Victoria, Australia), Jerry Meehl (National Center for Atmospheric Research, Boulder, CO USA), Model and Data Group (Max Planck Institute for Meteorologie, Hamburg, Germany), Erich Roeckner (Max Planck Institute, Hamburg, Germany), and Ron Stouffer (Geophysical Fluid Dynamics Laboratory, Princeton, MA USA). The views expressed herein are those of the authors and do not necessarily represent those of the IBHE, USEPA, or the Illinois State Water Survey.

7. References

Barnett, T. P., 1999: Comparison of near-surface air temperature variability in 11 coupled global climate models. *J. Climate*, **12**, 511-518.

Boer, G.J., G. Flato, and D. Ramsden, 2000: A transient climate change simulation with greenhouse gas and aerosol forcing: projected climate to the twenty-first century. *Climate Dyn*., **16**, 427-450.

Bosilovich, M. G. and S.D. Schubert, 2002: Water vapor tracers as diagnostics of the regional hydrologic cycle**.** *J. Hydrometeorology*, 3, 149–165.

Boville, B.A., and P.R. Gent, 1998: The NCAR Climate System Model, Version One. *J.Climate,* **11**, 1115-1130.

Covey, C., A. Abe-Ouchi, G.J. Boer, B.A. Boville, U. Cubasch, L. Fairhead, G.M. Flato, H. Gordon, E. Guilyardi, X. Jiang, T.C. Johns, H. Le Treut, G. Madec, G.A. Meehl, R. Miller, A. Noda, S.B. Power, E. Roeckner, G. Russell, E. K. Schneider, R.J. Stouffer, L. Terray, and J.-S. von Storch, 2000: The seasonal cycle in coupled ocean-atmosphere general circulation models. *Clim. Dyn*., 17, 775-787.

Covey, C., K.M. AchutaRao, U. Cubasch, P. Jones, S.J. Lambert, M.E. Mann, T.J. Phillips, K.E. Taylor, 2003: An overview of results from the Coupled Model Intercomparison Project. *Global and Planetary Change,* 37, 103-133.

Delworth, T.L., and T.R. Knutson, 2000: Simulation of early 20th century global warming. *Science*, **287 (5461)**, 2246-2250.

Dirmeyer, P. A., K. L. Brubaker, 1999: Contrasting evaporative moisture sources during the drought of 1988 and the flood of 1993. *J. Geophys. Res.,* 104, 19383-19398, 10.1029/1999JD900222.

Flato, G.M., G.J. Boer, W.G. Lee, N.A. McFarlane, D. Ramsden, M.C. Reader, and A.J. Weaver, 2000: The Canadian Centre for Climate Modelling and Analysis global coupled model and its climate. *Climate Dyn*., **16**, 451-467.

Flato, G.M., and G.J. Boer, 2001: Warming asymmetry in climate change simulations. *Geophys. Res. Lett.*, 28, 195-198, 10.1029/2000GL012121.

Folland, C.K., T.R. Karl, J.R. Christy, R.A. Clarke, G.V. Gruza, J. Jouzel, M.E. Mann, J. Oerlemans, M.J. Salinger, and S.-W. Wang, 2001: Observed climate variability and change. In: *Climate Change 2001: The Scientific Basis. Contributions of Working Group 1 to the Third Assessment Report of the Intergovernmental Panel on Climate Change* [Houghton, J.T., Y. Ding, D.J. Griggs, M. Noguer, P.J. van der Linden, X. Dai, K. Maskell, and C.A. Johnson (eds.)]. Cambridge University Press, Cambridge, United Kingdom and New York, NY, USA, 881 pp.

Gates, W. L., J. Boyle, C. Covey, C. Dease, C. Doutriaux, R. Drach, M. Fiorino, P. Gleckler, J. Hnilo, S. Marlais, T. Phillips, G. Potter, B. Santer, K. Sperber, K. Taylor and D. Williams, 1998: An overview of the results of the Atmospheric Model Intercomparison Project (AMIP I). *Bull. Amer. Meteor. Soc.*, **73**, 1962-1970.

Gordon, C., C. Cooper, C.A. Senior, H.T. Banks, J.M. Gregory, T.C. Johns, J.F.B. Mitchell, and R.A. Wood, 2000: The simulation of SST, sea ice extents and ocean heat transports in a version of the Hadley Centre copled model without flux adjustments. *Climate Dyn*., **16**, 147-168.

Gordon, H.B., and S.P. O'Farrell, 1997: Transient climate change in the CSIRO coupled model with dynamic sea ice. *Mon. Wea. Rev*., **125**, 875-907.

Gutowski, W.J., F.O. Otieno, R.W. Arritt, E.S. Takle, Z. Pan, 2004: Diagnosis and attribution of a seasonal precipitation deficit in a U.S. regional climate simulation**.** *J. Hydrometeorology*, 5, 230–242.

Hirst, A.C., S.P. O'Farrell, And H.B. Gordon, 2000: Comparison of a coupled ocean-atmosphere model with and without oceanic eddy-induced advection. 1. Ocean spin-up and control integrations. *J. Climate*, **13**, 139-163.

Johns, T.C., R.E. Carnell, J.F. Crossley, J.M. Gregory, J.F.B. Mitchell, C.A. Senior, S.F.B. Tett, and R.A. Wood, 1997: The second Hadley Centre coupled ocean-atmosphere GCM: Model description, spinup and validation. *Climate Dyn*., **13**, 103-134.

Kanamitsu, M., W. Ebisuzaki, J. Woollen, S.-K. Yang, J.J. Hnilo, M. Fiorino, and G.L. Potter, 2002: The NCEP-DOE AMIP-II reanalysis (R-2). *Bull. Amer. Meteor. Soc.*, **83**, 1631-1643.

Lambert, S.J. and G.J. Boer, 2001: CMIP1 evaluation and intercomparison of coupled climate models. *Clim. Dyn*., 17, 83-106.

Legutke, S. and R. Voss, 1999: The Hamburg Atmosphere-Ocean Coupled Circulation Model ECHO-G. Technical report, No. 18, German Climate Computing Centre (DKRZ), Hamburg, 62 pp. (Available from Deutsches Klimarechenzentrum, Bundesstrasse 55, D-20146 Hamburg, Germany, or online at http://www.mad.zmaw.de/Pingo/reports/ReportNo.18.pdf)

Liang, X.-Z., K.E. Kunkel, and A.N. Samel, 2001a: Development of a regional climate model for U.S. Midwest applications. Part 1: Sensitivity to buffer zone treatment. *J. Climate*, **14**, 4363-4378.

Liang, X.-Z., L. Li, K.E. Kunkel, M. Ting, and J. X. L. Wang, 2004: Regional climate model simulation of U.S. precipitation during 1982-2002 Part I: Annual cycle. *J. Climate*, in press.

Liang, X.-Z., W.-C. Wang, and A.N. Samel, 2001b: Biases in AMIP model simulations of the east China monsoon system. *Climate Dynamics*, **17**, 291-304.

Liu, P., G.A. Meehl, and G. Wu, 2002: Multi-model trends in the Sahara induced by increasing CO2. Geophys. Res. Lett., 29, 1881, doi: 10.1029/2002GL015923.

Meehl, G.A., G.J. Boer, C. Covey, M. Latif, and R.J. Stouffer, 2000: The Coupled Model Intercomparison Project (CMIP). *Bull. Amer. Meteor. Soc*., **81**, 313--318.

Mo, K. C., R.W. Higgins, 1996: Large-scale atmospheric moisture transport as evaluated in the NCEP/NCAR and the NASA/DAO reanalyses**.** *J. Climate*, 9, 1531–1545.

Rayner, N.A., E.B. Horton, D.E. Parker, C.K. Folland, and R.B. Hackett, *Version 2.2 of the global sea-ice and sea surface temperature data set, 1903-1994*, Climate Technical Note 74, Hadley Centre for Climate Prediction and Research, UK Meteorological Office, 1996.

Reynolds, R. W. and T. M. Smith, 1994: Improved global sea surface temperature analyses using optimum interpolation. *J. Climate,* **7,** 929–948.

Roeckner, E., J.M. Oberhuber, A Bacher, M. Christoph, and I. Kirchner, 1996: ENSO variability and atmospheric response in a global coupled atmosphere-ocean GCM. *Climate Dyn*., **12**, 737-754.

Washington, W.M., J.M. Weatherly, G.A. Meehl, A.J. Semtner, Jr., T.W. Bettge, A.P. Craig, W.G. Strand, J. Arblaster, V.B. Wayland, R. James, and Y. Zhang, 2000: Parallel Climate Model (PCM) control and transient simulations. *Climate Dyn*., **16**, 755-774.

Table Captions

Table 1. Characteristics of CMIP Models

Figure Captions

Figure 1. Solid box outlines the central U.S. (CUS) area of study. Dashed boxes outline two areas for which indexes were calculated: a low-level jet area (LLJ) and an upper level jet stream area (UJ).

Figure 2. Map of R-2 (1979-1995) wind flow at a level of 850 hPa for (a) winter, (b) spring, (c) summer, and (d) fall and at a level of 200 hPa for (e) winter, (f) spring, (g) summer, and (h) fall. Arrows indicated wind direction and speed (length of arrow). Contour lines indicate speed (m s^{-1}) with shading for speeds in excess of 5 m s^{-1} for 850 hPa and 30 m s^{-1} for 200 hPa.

Figure 3. Maps of correlation coefficient for 1979-1995 between seasonal time series of the R-2 southerly component of the wind speed at 850 hPa and COOP precipitation in the CUS region (Fig. 1) for (a) winter, (b) spring, (c) summer, and (d) fall and between seasonal time series of the R-2 westerly component of the wind speed at 200 hPa and COOP precipitation in the central U.S. for (e) winter, (f) spring, (g) summer, and (h) fall. Solid (dashed) lines denote positive (negative) correlations. Absolute values of the correlation coefficient exceeding 0.28 are statistically significant at the 95% level of confidence.

Figure 4. Annual and seasonal precipitation in the CUS region (Fig. 1) for the COOP data (1979-1995), the control simulations of the CMIP models, and model means of all CMIP and AMIP models. For the AMIP results, the maximum and minimum model values are denoted by the vertical line.

Figure 5. (a) Southerly wind component (m s^{-1}) and (b) specific humidity at 850 hPa in the LLJ region (Fig. 1) for the 4 seasons for CMIP models (last 30 years of control run) and R-2 data for the period 1979-1995. Model mean is also displayed.

Figure 6. Correlation coefficients for 4 seasons for CMIP models between time series for (a) CUS region (Fig. 1) model precipitation and model southerly wind component in the LLJ region (Fig. 1) and (b) CUS region (Fig. 1) model precipitation and model westerly component of the wind speed at 200 hPa in the UJ region (Fig. 1). Model mean is also shown.

Figure 7. Annual and seasonal mean surface air temperature (°C) in the CUS region (Fig. 1) for the COOP data (1979-1995), the control simulations of the CMIP models, and model means of all CMIP and AMIP models. For the AMIP results, the maximum and minimum model values are also denoted by the vertical line.

Figure 8. Precipitation changes in the transient runs of the CMIP models for the CUS region (Fig. 1). The change is the difference between the average of years 65-75 in the transient run and the average of the last 30 years of the control run. Also shown is the maximum and minimum values (expressed as a deviation from the mean) of a 11-year running average of the control run and of a 11-yr running average of the 20th Century (1900-1999) COOP data for CUS precipitation for the four seasons.

Figure 9. Surface air temperature changes (°C) in the transient runs of the CMIP models for the CUS region (Fig .1). The change is the difference between the average of years 65-75 in the transient run and the average of the last 30 years of the control run. Also shown is the maximum and minimum values (expressed as a deviation from the mean) of a 11-year

running average of the control run and of a 11-yr running average of the 20th Century (1900-1999) COOP data for central US surface air temperature for the four seasons.

Figure 10. CMIP model composite maps of wind flow at a level of 850 hPa for (a) winter, (b) spring, (c) summer, and (d) fall and at a level of 200 hPa for (e) winter, (f) spring, (g) summer, and (h) fall. Arrows indicated wind direction and speed (length of arrow). Contour lines indicate speed (m s^{-1}) with shading for speeds in excess of 5 m s^{-1} for 850 hPa and 30 m s^{-1} for 200 hPa.

Figure 11. AMIP model composite maps of correlation coefficient between model mean values of southerly component of the wind speed at 850 hPa and precipitation in the central U.S. for (a) winter, (b) spring, (c) summer, and (d) fall and between model mean values of westerly component of the wind speed at 200 hPa and precipitation in the central U.S. for (e) winter, (f) spring, (g) summer, and (h) fall. Solid (dashed) lines denote positive (negative) correlations. Correlation coefficients exceeding an absolute value of 0.25 are statistically significant at the 95% level of confidence.

Table 1. Characteristics of CMIP Models

	Flux Adjustment	Control Run CO_2 (ppm)	Transient Run Year 70 CO2 (ppm)	Solar Constant (Wm-2)	No. Vertical Levels	Bottom, Top (hPa)	Key References
CCCMA	Yes, heat, water	330	662	1370	10	980, 5	Flato et al. 2000 Flato and Boer, 2001 Boer et al. 2000
NCAR CSM	No	355	712	1367	18	992, 3	Boville and Gent 1998
CSIRO	Yes, heat, water, momentum	330	662	1367	9	979, 21	Gordon and O'Farrell, 1997; Hirst et al., 2000
ECHAM4-OPYC	Yes, heat, water	353	708	1365	19	996, 10	Roeckner et al., 1996
ECHO-G	Yes, heat, water				19	996, 10	Legutke and Voss, 1999
GFDL	Yes, heat, water	360	722	1365	14	997, 15	Delworth and Knutson, 2000
HadCM2	Yes, heat, water	322.6	648	1365	19	997, 5	Johns et al., 1997
HadCM3	No	289.6	581	1365	19	997, 5	Gordon et al., 2000
DOE PCM	No	355	712	1367	18	992, 3	Washington et al ., 2000

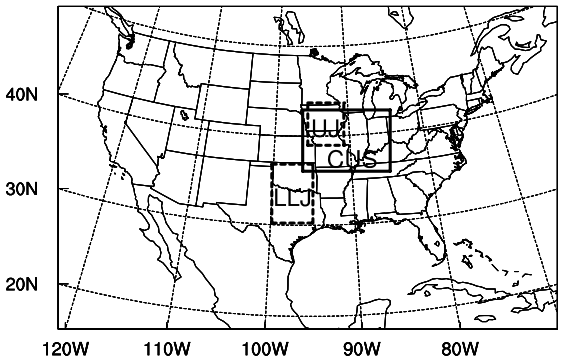
40N
30N
20N
120W
110W
100W
90W
80W
UJJ
CNS
LLJ

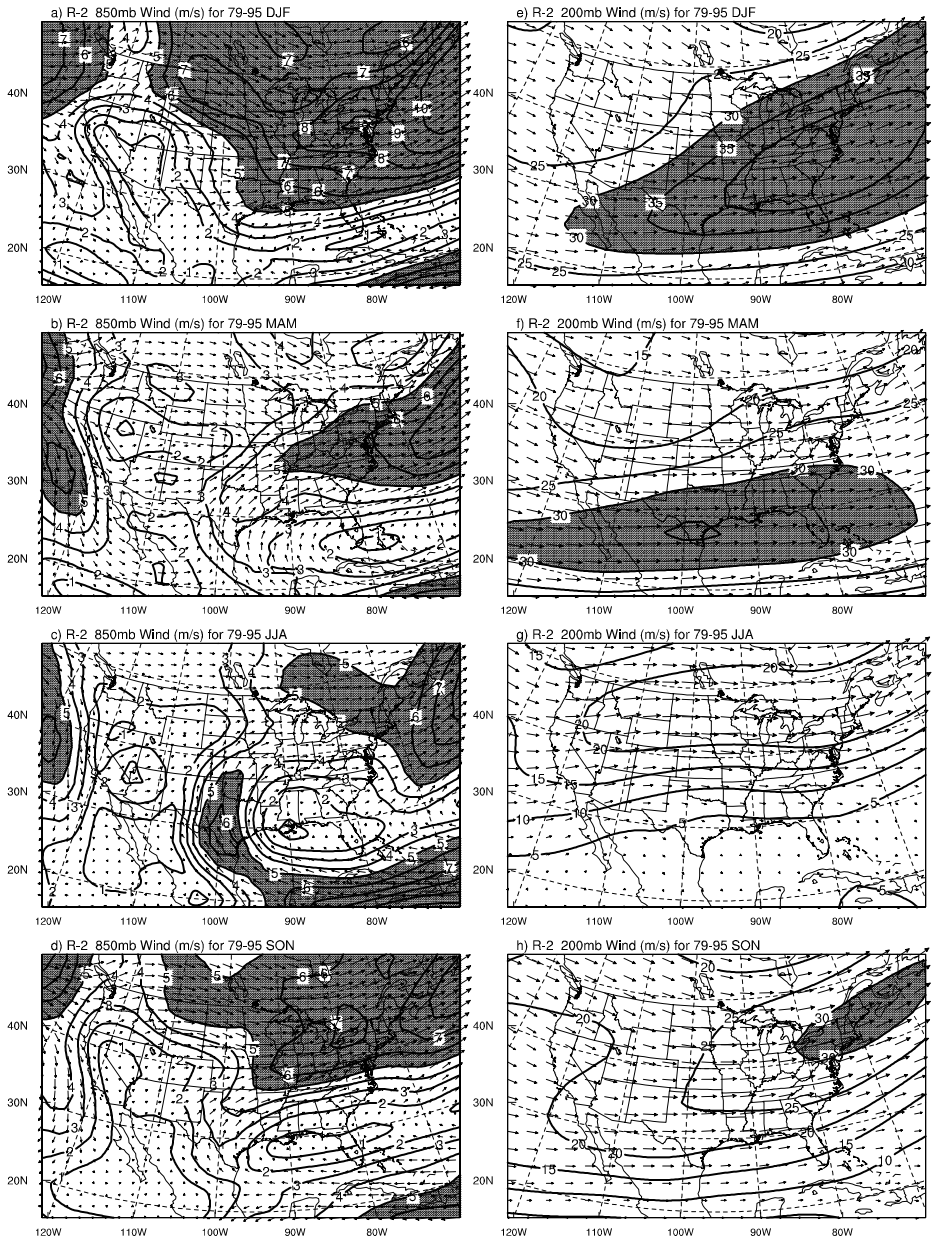
a) R-2 850mb Wind (m/s) for 79-95 DJF
e) R-2 200mb Wind (m/s) for 79-95 DJF
b) R-2 850mb Wind (m/s) for 79-95 MAM
f) R-2 200mb Wind (m/s) for 79-95 MAM
c) R-2 850mb Wind (m/s) for 79-95 JJA
g) R-2 200mb Wind (m/s) for 79-95 JJA
d) R-2 850mb Wind (m/s) for 79-95 SON
h) R-2 200mb Wind (m/s) for 79-95 SON
40N
30N
20N
120W
110W
100W
90W
80W

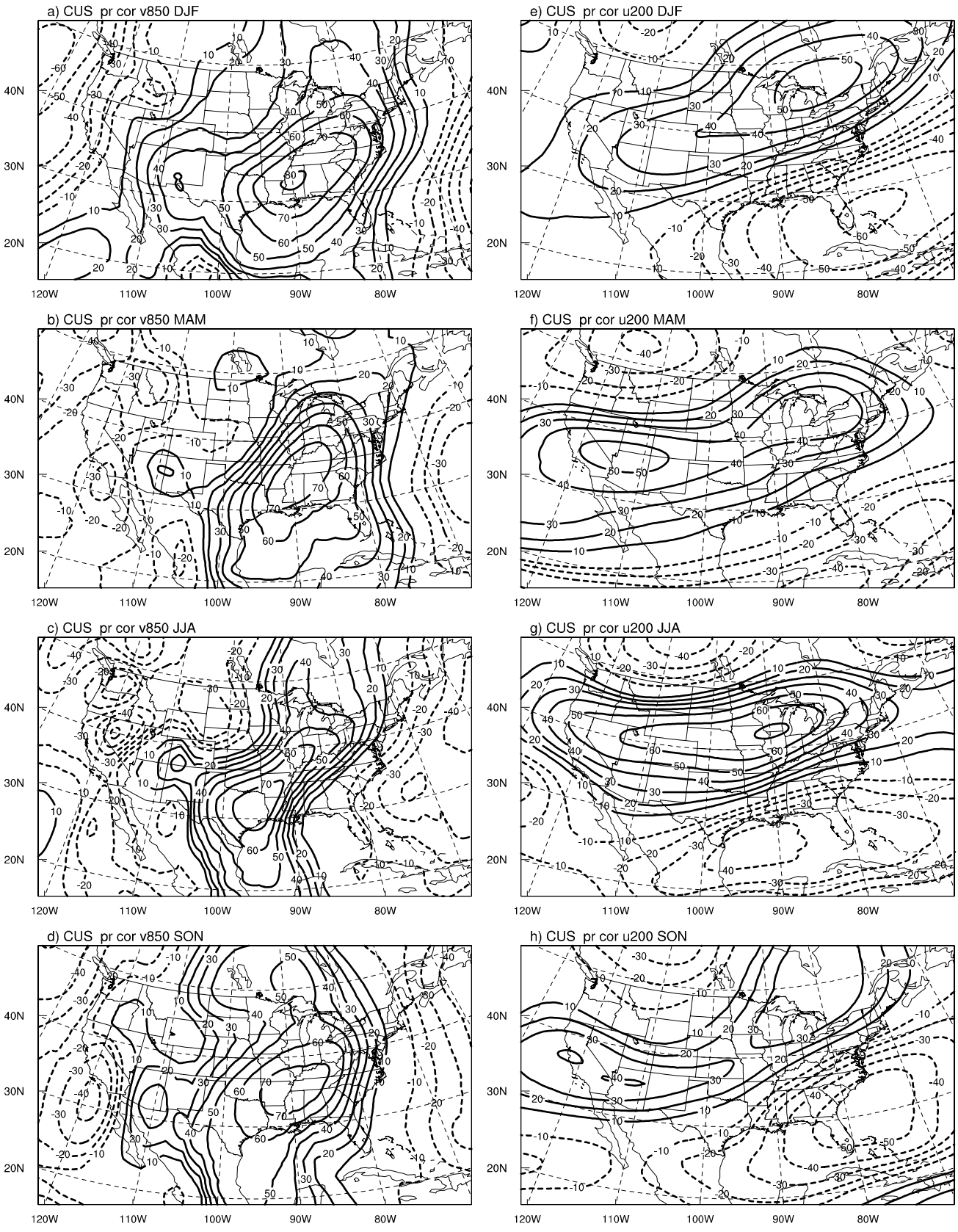
a) CUS pr cor v850 DJF
e) CUS pr cor u200 DJF
b) CUS pr cor v850 MAM
f) CUS pr cor u200 MAM
c) CUS pr cor v850 JJA
g) CUS pr cor u200 JJA
d) CUS pr cor v850 SON
h) CUS pr cor u200 SON
40N
30N
20N
120W
110W
100W
90W
80W

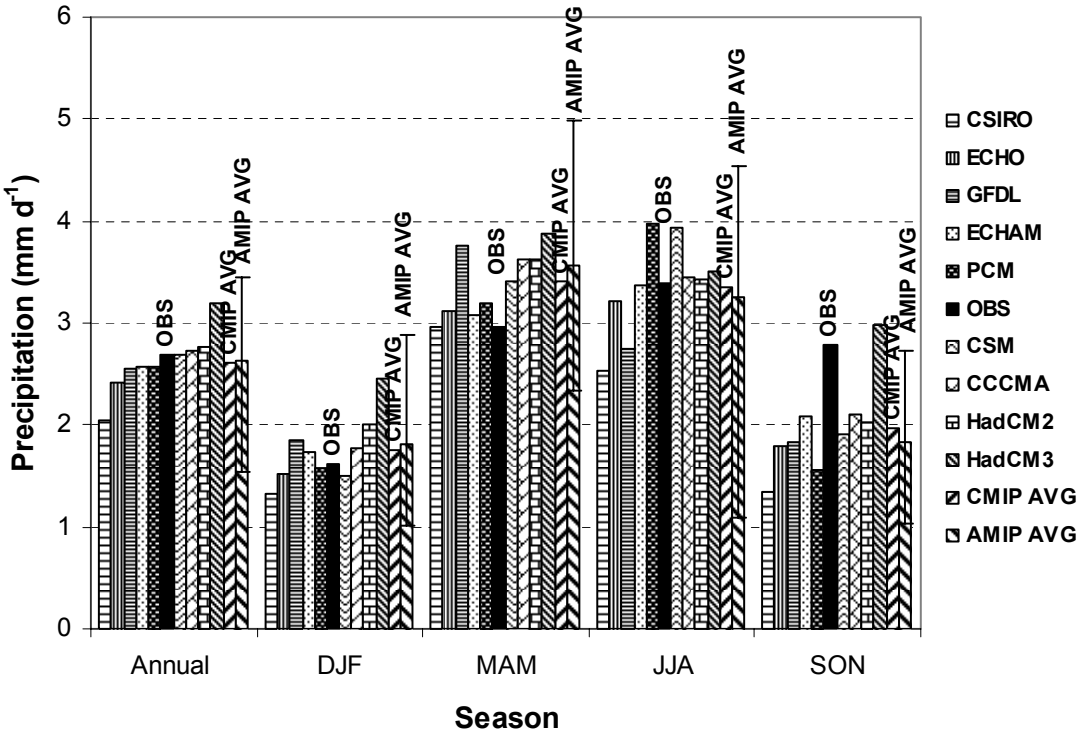
Precipitation (mm d-1)
6
5
4
3
2
1
0
Annual
DJF
MAM
JJA
SON
Season
OBS
CMIP AVG
AMIP AVG
CSIRO
ECHO
GFDL
ECHAM
PCM
OBS
CSM
CCCMA
HadCM2
HadCM3
CMIP AVG
AMIP AVG

Figure 4

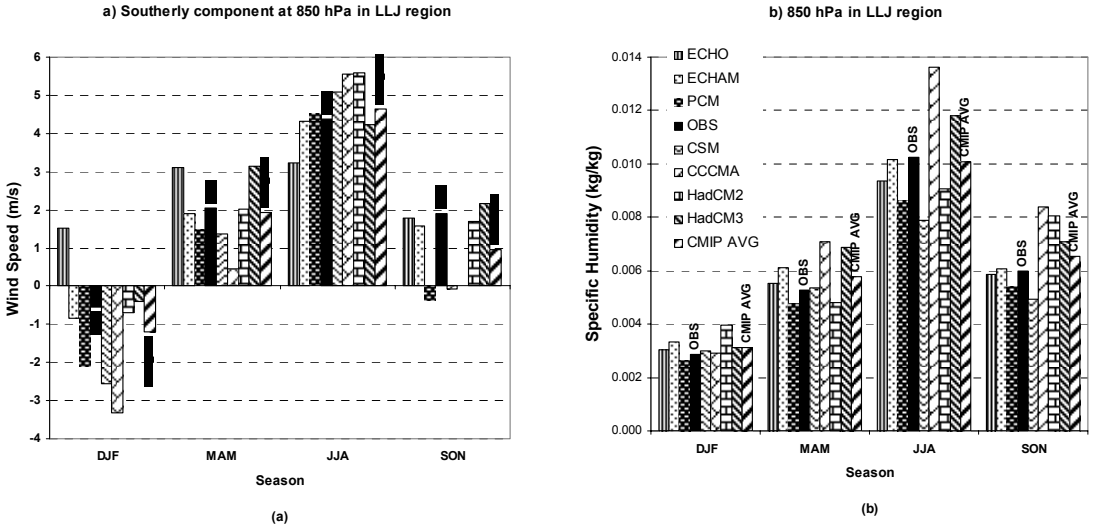
a) Southerly component at 850 hPa in LLJ region
Wind Speed (m/s)
6
5
4
3
2
1
0
-1
-2
-3
-4
DJF
MAM
JJA
SON
Season
(a)
b) 850 hPa in LLJ region
Specific Humidity (kg/kg)
0.014
0.012
0.010
0.008
0.006
0.004
0.002
0.000
ECHO
ECHAM
PCM
OBS
CSM
CCCMA
HadCM2
HadCM3
CMIP AVG
OBS
CMIP AVG
DJF
MAM
JJA
SON
Season
(b)

Figure 5

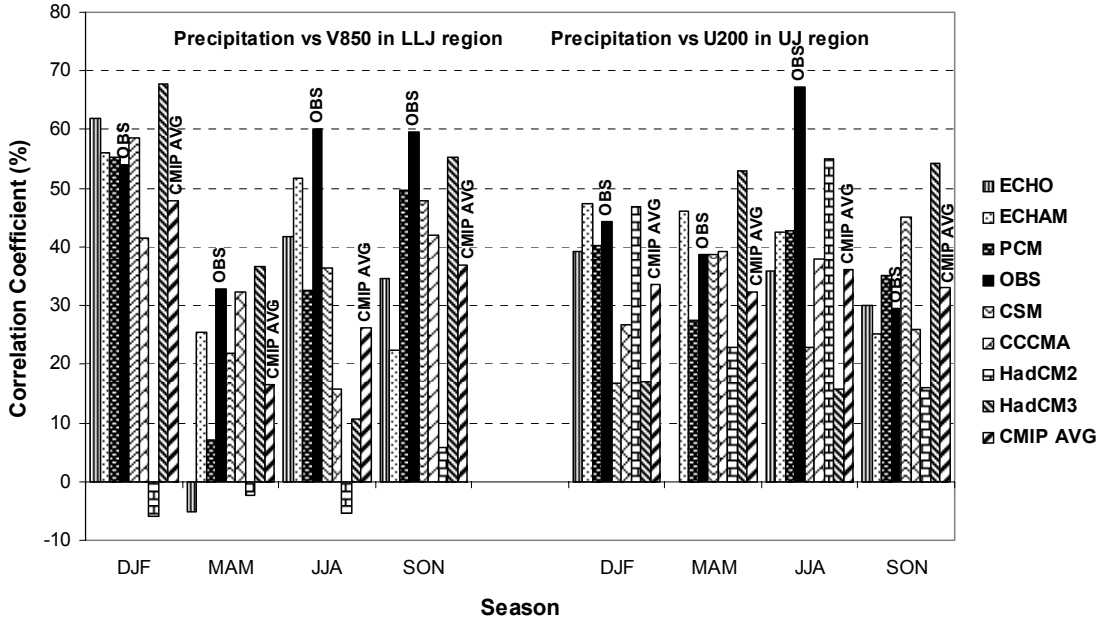
Precipitation vs V850 in LLJ region
Precipitation vs U200 in UJ region
Correlation Coefficient (%)
80
70
60
50
40
30
20
10
0
-10
DJF
MAM
JJA
SON
Season
OBS
CMIP AVG
ECHO
ECHAM
PCM
OBS
CSM
CCCMA
HadCM2
HadCM3
CMIP AVG

Figure 6

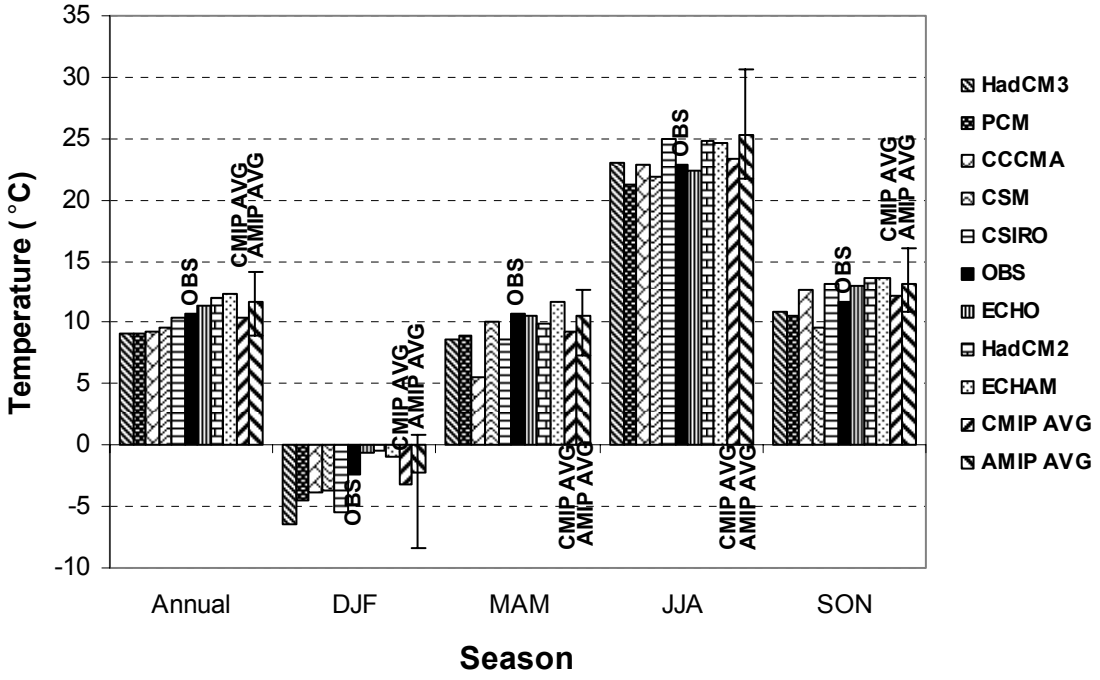
35
30
25
20
15
10
5
0
-5
-10
Temperature (°C)
OBS
CMIP AVG
AMIP AVG
Annual
DJF
MAM
JJA
SON
Season
HadCM3
PCM
CCCMA
CSM
CSIRO
OBS
ECHO
HadCM2
ECHAM
CMIP AVG
AMIP AVG

Figure 7

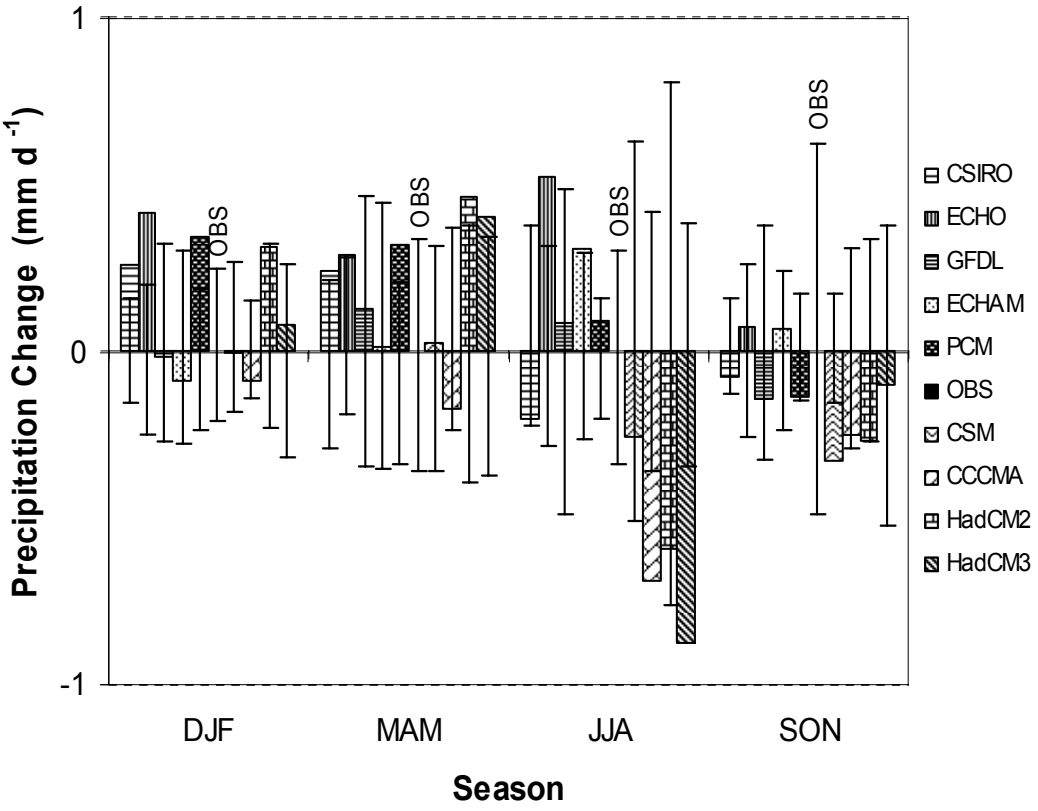
1
0
-1
Precipitation Change (mm d -1)
OBS
OBS
OBS
OBS
DJF
MAM
JJA
SON
Season
CSIRO
ECHO
GFDL
ECHAM
PCM
OBS
CSM
CCCMA
HadCM2
HadCM3

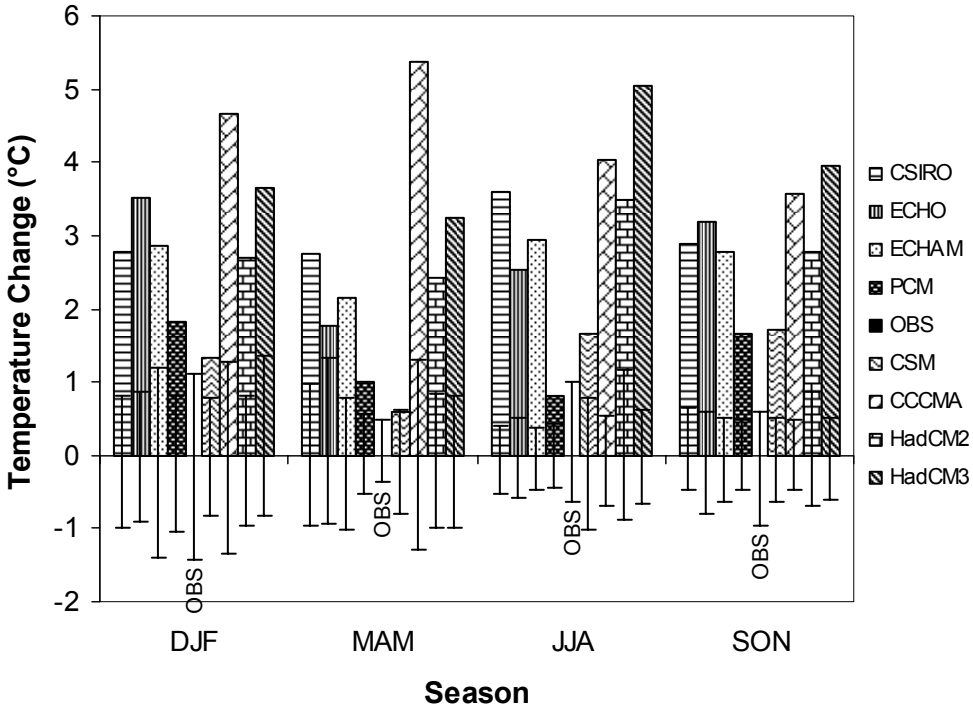
6
5
4
3
2
1
0
-1
-2
Temperature Change (°C)
OBS
OBS
OBS
OBS
DJF
MAM
JJA
SON
Season
CSIRO
ECHO
ECHAM
PCM
OBS
CSM
CCCMA
HadCM2
HadCM3

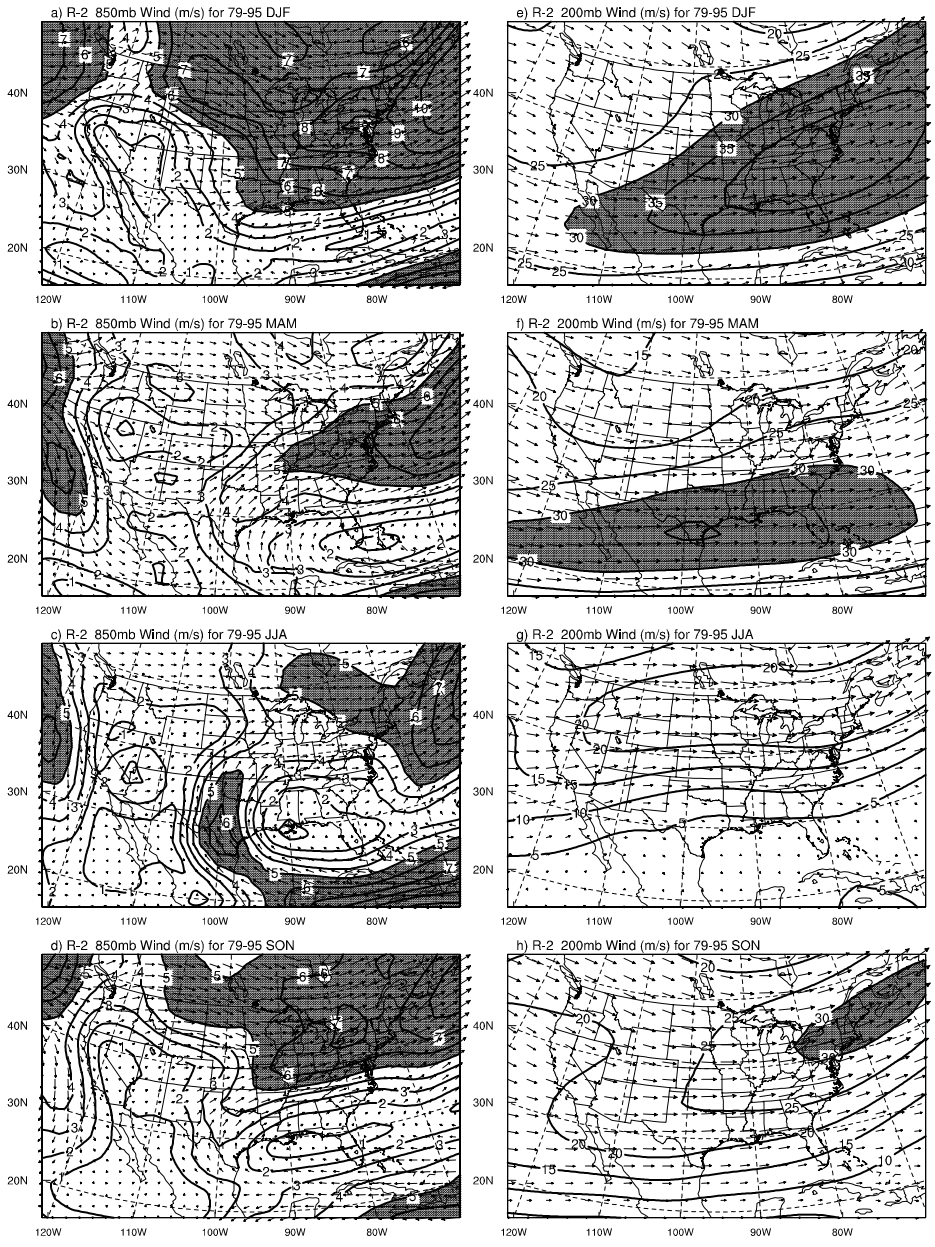
a) R-2 850mb Wind (m/s) for 79-95 DJF
e) R-2 200mb Wind (m/s) for 79-95 DJF
b) R-2 850mb Wind (m/s) for 79-95 MAM
f) R-2 200mb Wind (m/s) for 79-95 MAM
c) R-2 850mb Wind (m/s) for 79-95 JJA
g) R-2 200mb Wind (m/s) for 79-95 JJA
d) R-2 850mb Wind (m/s) for 79-95 SON
h) R-2 200mb Wind (m/s) for 79-95 SON
40N
30N
20N
120W
110W
100W
90W
80W

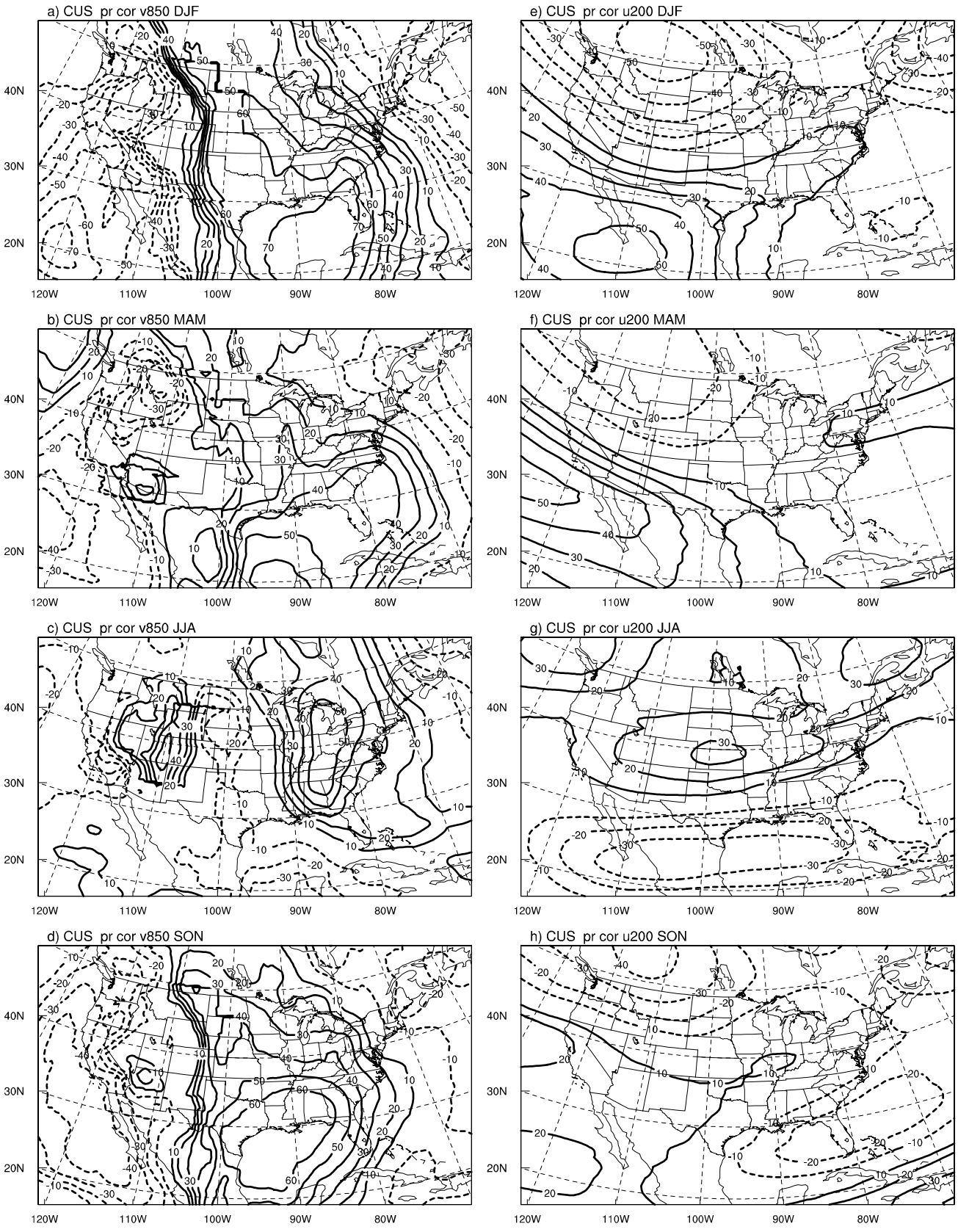
a) CUS pr cor v850 DJF
e) CUS pr cor u200 DJF
b) CUS pr cor v850 MAM
f) CUS pr cor u200 MAM
c) CUS pr cor v850 JJA
g) CUS pr cor u200 JJA
d) CUS pr cor v850 SON
h) CUS pr cor u200 SON
40N
30N
20N
120W
110W
100W
90W
80W